

TECHNICAL UNIVERSITY OF CLUJ-NAPOCA

ACTA TECHNICA NAPOCENSIS

Series: Applied Mathematics, Mechanics, and Engineering Vol. 68, Issue Special I, May, 2025

RESEARCH ON THE NUMERICAL MODELING OF THE INCREMENTAL PLASTIC DEFORMATION PROCESS USING A HEMISPHERICAL TOOL

Emanuel BĂDULESCU, Daniela Monica IORDACHE, Eduard Laurențiu NIȚU, Claudiu BĂDULESCU

Abstract: This study presents the numerical modeling of incremental plastic deformation using a hemispherical tool on AA6061 aluminum alloy. A finite element model was developed in ABAQUS, using the explicit method. The thermo-mechanical behavior of the material was defined by the Johnson-Cook law, the modeling of thermal phenomena was based on an adiabatic approach, and the simulation time was reduced by using mass scaling. Validation, based on comparing the simulation results with experimental deformation forces and temperatures, revealed similar trends, although some differences in the maximum values appeared due to modeling assumptions. The analysis of deformation forces, temperatures, 3D shape evolution and plastic equivalent strain provided key information on the SPIF process. Key points identified include the onset of plastic deformation, stabilization of forces, and temperature during the process. Keywords: Incremental sheet forming, hemispherical tool. FEM, AA6061-T6

1. INTRODUCTION

Incremental sheet forming (ISF) is a process used to gradually deform sheets, enabling the fabrication of complex parts without rigid dies. This method is employed in the automotive, aerospace, and biomedical industries due to its flexibility and reduced costs for small-series production and prototypes [1-8]. However, the process's complexity requires a thorough understanding of material behavior under deformation and technological parameters. Among the materials used in ISF, aluminum and its alloys are frequently utilized due to their excellent formability. Additionally, the demand for aluminum components in the automotive and aerospace industries is steadily increasing as efforts to reduce vehicle weight intensify.

Numerical simulation, particularly using Finite Element Analysis (FEA), is employed to understand and optimize the ISF process. It enables stress and strain distribution analysis, minimizes defects such as excessive thinning, and improves surface quality, facilitating ISF adoption across various industrial applications. [1], [2], [4], [9-17].

Khan and Pradhan (2019) used the ANOVA method to optimize SPIF process parameters for AA8011 aluminum sheets [13]. Simulations realised with ANSYS showed a good correlation with experimental results, highlighting that reducing the forming step improved thickness uniformity and prevented excessive thinning. It was also found that thickness reduction is significantly influenced by axial depth and wall angle. The SPIF process can efficiently form truncated cones with wall angles of up to 65° and depths of 30 mm.

Numerical simulations, closely linked to experimental validations, confirmed the accuracy of thickness modeling and provided detailed predictions of material thinning [3], [15]. Zeradam and Krishnaiah (2020) conducted numerical simulations and experimental tests on steel sheets. The sine law was used to predict thinning, and ABAQUS simulations correlated well with experimental data. The precision of material thinning predictions during the process was enhanced by integrating simulations with theoretical methods such as the sine law.

Kumar (2024) reviewed factors affecting surface roughness in the ISF process [4]. The

study suggested optimizing tool trajectories and using lubricants to reduce roughness. Numerical simulations indicated that lowering the tool feed rate improved surface quality but increased forming time.

Vosniakos et al. (2021) studied the SPIF process applied to turbine blade components made of AA6082 [18]. Simulations conducted with LS-DYNA were validated by comparing thickness, deformation, and geometric deviations using 3D scans. Numerical results indicated that reducing spindle speed improved the dimensional accuracy of asymmetric parts, while wall angles and step-down parameters significantly affected stress and thickness.

Chang et al. (2025) investigated the influence of friction and vibrations on surface quality in ISF for aluminum alloys such as AA5251 and AA6082 [19]. Analytical models and simulations demonstrated that high-amplitude vibrations reduced the friction coefficient and enhanced surface microhardness.

Advanced numerical simulations using multitooling, multi-point systems with layered sheets, or adaptive mesh concepts have reduced forming time and minimized pillow and springback defects in aluminum parts, improving dimensional accuracy [14], [20], [21].

The analyzed studies show that numerical simulation plays a critical role in ISF process development, offering numerous advantages. First, simulation enables accurate prediction of stress and strain distributions, helping prevent defects such as excessive thinning or cracking. Second, it significantly reduces the time and costs of physical experimentation, providing a virtual testing environment for process parameter optimization.

The diversity of software tools reflects the varied requirements of the ISF process, from deformation simulation and stress analysis to toolpath generation and process optimization. ABAQUS, LS-DYNA, and ANSYS [14], [16], [21], [22] are preferred for detailed analysis of deformation behavior, while software like CATIA and Mastercam is used for toolpath generation.

This study details the research to develop a numerical model for simulating the Incremental Sheet Forming (ISF) process using AA6061 aluminum alloy sheets and a hemispherical tool. The numerical model employs the finite element

method (FEM) and is implemented using ABAQUS software, utilizing the explicit method to emphasize plastic deformation phenomena. The validation of the numerical model involved analyzing the deformation forces and temperatures during the process and comparing them with experimental data.

2. EXPERIMENTAL METHODOLOGY

The geometry of the part produced by ISF is characterized by a truncated cone (TC) type, as shown in Figure 1:

- the large diameter of the cone, D = 96 [mm];
- the height of the cone, H = 25 [mm];
- the angle of inclination of the wall $\alpha = 45$ [°].

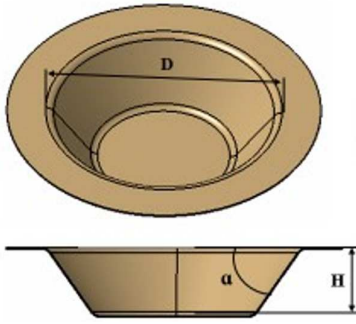


Fig. 1. The geometry of the part manufactured by ISF.

The part is made from 1 mm thick AA6061-T6 aluminum alloy sheet, commonly used in automotive and aerospace industries. This material is particularly valued for its ability to be formed into exterior or structural components through cold plastic deformation. This alloy's effective chemical composition and mechanical properties are summarized in Table 1 and Table 2, respectively.

Table 1

Chemical composition of AA6061-T6 aluminum alloy						lloy.				
Chemical element	Si	Cu	Mg	Cr	Fe	Mn	Zn	Ti	Other	Al
wt%	1.52	0.38	1.59	0.27	0.65	0.19	0.1	0.04	1.05	94.21

The single-point incremental forming method (SPIF) used in the research is shown in Figure 2.

The technological parameters of the SPIF utilized in this study are as follows:

- tool speed n = 2000 [rot/min],
- tool feed rate in the XOY working plane v_a = 1000 [mm/min],
- incremental step on the Z axis $\Delta z = 0.3$ [mm].

Table 2
Mechanical properties of AA6061-T6 aluminum allov.

Mechanical property Unit Value Hardness HB 95 Tensile strength (Rm) MPa 345		
Mechanical property	Unit	Value
Hardness	HB	95
Tensile strength (Rm)	MPa	345
Yield strength (Rp0.2)	MPa	270
Elongation (At)	%	14

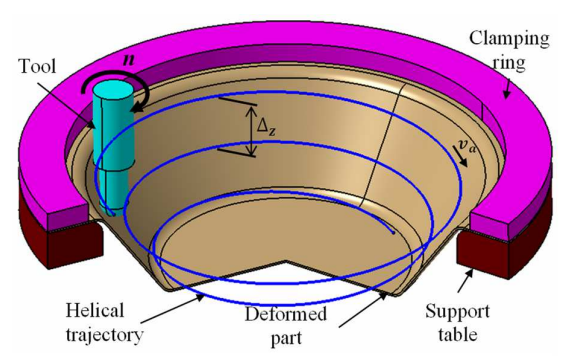


Fig. 2. SPIF processing scheme.

A rigid tool with a hemispherical head of radius R = 10 mm was made of HSS tool steel, as shown in Figure 3.

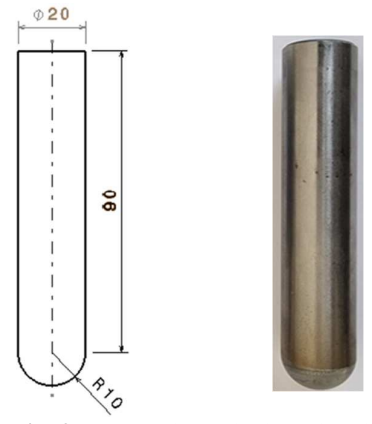


Fig. 3. The hemispherical head tool.

The experiments were conducted using a specially designed experimental stand mounted on a DMG MORI EcoMill 70 numerically controlled milling machine. As shown in Figure 4, the stand consists of several components: a device for orienting and clamping the blank, a dynamometer for measuring deformation forces, and a thermographic camera for monitoring temperatures during the process. The workpiece orientation and clamping device is positioned centrally on the force-measuring dynamometer and features a rigid construction. It includes a slot that provides the thermal imaging camera access to the part's exterior during the incremental deformation process.



Fig. 4. Experimental stand: 1 - Dynamometer; 2 - Thermographic camera; 3 - Device for orienting and fixing the workpiece; 4 - Workpiece clamping ring; 5 - Workpiece (sheet metal); 6 - Tool.

To measure the deformation force, we used a dynamometer, Meßsysteme model K3D160. This device has a maximum measurement capacity of ±20 kN and a precision of ±0.02 kN. It enabled us to measure the components of the deformation force along the X, Y, and Z axes, with the Z axis representing the axis of symmetry of the part. The force measurement data were acquired using the National Instruments cDAQ-9171 uni-modular platform with the NI9237 acquisition module, and the data collection was conducted through Matlab R2023 software via the Analog Input Recorder module. The data acquisition frequency was set to 2500 Hz.

The thermography technique was employed to measure temperatures during the process using the Optris PI400i thermal imaging camera, which has a measurement accuracy of ±2°C and an image acquisition frequency of 40 Hz. The thermographic images were processed with MATLAB software to identify the maximum temperature. The thermographic chamber and the access slot to the deformed part were covered with aluminum foil to accurately measure radiation from the heat released during the incremental deformation process. Additionally, the underside of the sheet metal was painted with capable heat-resistant black paint, withstanding temperatures of up to 800°C (see Fig. 5).



Fig. 5. Workpieces (sheet metal) painted on the underside with heat-resistant paint.

3. NUMERICAL MODEL DEVELOPMENT

The numerical model developed to simulate the SPIF process has been designed to match the experimental setup, as illustrated in Figure 6.

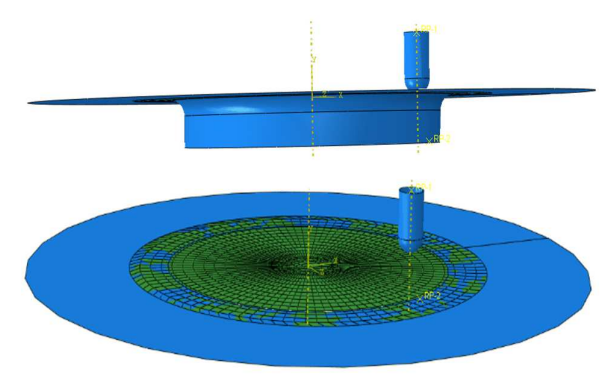


Fig. 6. Numerical model of SPIF

This model simulates the deformation of an AA6061-T6 aluminum sheet into a truncated cone shape using a hemispherical tool with a radius of 10 mm. The Abaqus software was used to create and analyze the numerical model. The toolpath was generated in CATIA V5 and then integrated into Abaqus to ensure high accuracy.

The material was defined in Abaqus using the Johnson-Cook law, Eq. 1.

$$\sigma = [A + B(\varepsilon^n)] \left[1 + C \ln \left(\frac{\varepsilon}{\varepsilon_0} \right) \right]$$

$$\left[1 - \left(\frac{T - T_{room}}{T_{melt} - T_{room}} \right)^m \right]$$
(1)

where: σ is the Yield stress; ϵ , Plastic strain; ϵ , Strain rate; ϵ , Reference strain rate; T, Material temperature; T_{room} , Ambient temperature; T_{melt} , Material melting temperature; A, B, C, n, m, Material constants.

The physical properties of the material used in the simulation are presented in Table 3 [23], while the Johnson-Cook law parameters, Table 4, were determined experimentally using the methodology from [24].

Physical Properties of AA6061-T6.

Parameter Name	Unit	Value
Thermal Conductivity	$W/(m \cdot K)$	167
Density	g/mm³	2.7e-06
Elastic Modulus	MPa	68915
Poisson's Ratio	Dimensionless	0.339
Inelastic Heat Fraction	Dimensionless	0.95
Specific Heat	J/(kg·K)	893000

Table 4

Table 3

Johnson-Cook Parameters.

Parameter Name	Unit	Value
Initial Yield Stress (A)	MPa	285.8
Hardening Modulus (B)	MPa	331.6
Hardening Exponent (n)	Dimensionless	0.5657
Thermal Softening	Dimensionless	0.8263
Exponent (m)		
Melting Temperature	°C	600
Reference Temperature	°C	22
Strain Rate Sensitivity (C)	Dimensionless	0.0113
Reference Strain Rate	S^{-1}	0.00364

In the simulation of the SPIF process, the sheet is encastred at its edges, and the contact is defined between the tool and material surfaces using the Contact Pair method with a kinematic constraint. The friction coefficient used is 0.1, representative of the interaction between aluminum and the hemispherical tool.

The penalty method is employed to accurately model mechanical phenomena and maintain the correlation between simulation and experiment, contributing to the correct prediction of deformation, thinning, and the geometric accuracy of the formed part. Friction plays a crucial role in the simulation, influencing surface quality and force control during deformation.

For the discretization of the sheet, S4RT shell finite elements (1735 quadrilateral elements with reduced integration) and S3RT shell finite elements (24 triangular elements) were used.

4. RESULTS AND DISCUSSIONS

The experimental and simulation results of the deformation forces are presented in Figure 7. Analyzing these results reveals the following key aspects.

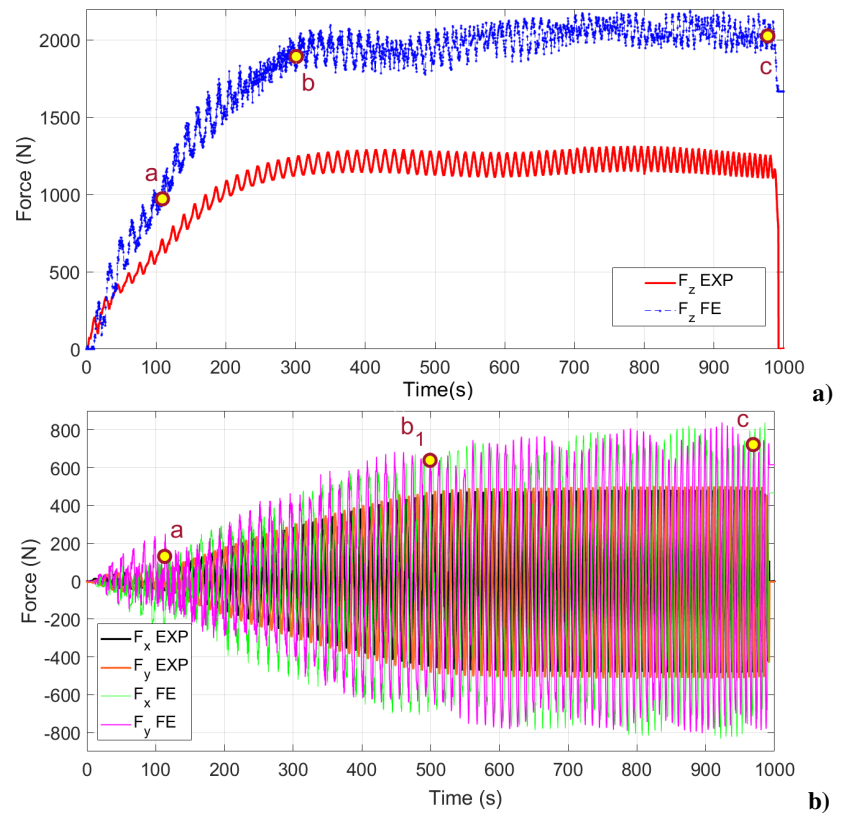


Fig. 7. Evolution of deformation forces: a) along the Z axis; b) along the X and Y axes.

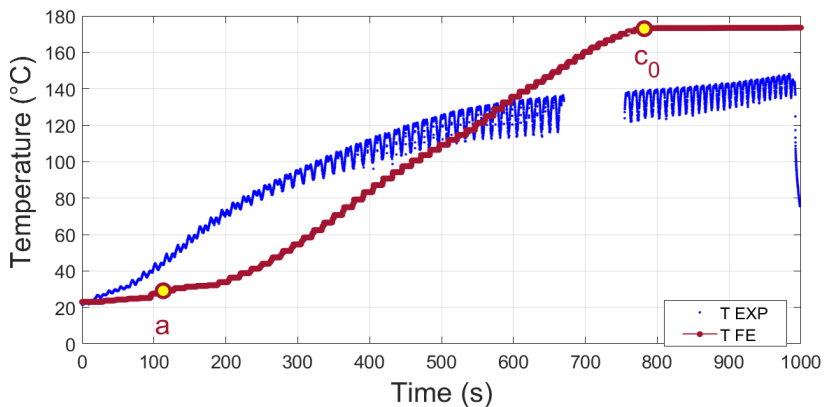


Fig. 8. Temperature evolution in the process.

The primary component of the deformation force acts in the Z-axis direction, which is the axis of symmetry for the part. This component has the largest magnitude because the tool presses down on the material along the Z-axis to induce plastic deformation. This process requires a significant force to overcome the material's yield stress and facilitate its plastic elongation. The progression of the force in the Z-direction is characterized by an initial increase, followed by a relatively stable phase:

At the beginning of the process, the tool interacts with the undeformed material, which has a high resistance to deformation. Once the elastic limit is exceeded, the material of the metal sheet enters the plastic region and experiences positive hardening, requiring greater forces for deformation. During this stage, friction between the tool and the material increases, as the contact surface between them becomes larger.

As the material begins to flow plastically, its resistance decreases, and the required

deformation force stabilizes. Additionally, the contact between the tool and the material becomes stable, and the friction levels out.

The deformation forces in the horizontal plane (along the X and Y axes) are symmetrical and are approximately three times smaller than the deformation force along the Z axis. The forces on the X and Y axes result from the lateral redistribution of material during deformation and from the friction between the tool and the material. As the tool advances, it pushes the material laterally, which is reflected in the forces acting on the X and Y axes. The evolution of these forces is similar to that of the deformation force in the Z axis, characterized by an initial increase followed by a relatively constant state.

The forces obtained through simulation exhibit shapes that are very similar to those determined experimentally. However, there are notable differences in their maximum values, with the simulated values being higher than those measured experimentally. The primary reasons for these discrepancies include: i) the use of a mass scaling strategy to reduce simulation time, which tends to generate higher forces than those obtained without this approach; ii) the Johnson-Cook law used to describe thermo-mechanical behavior may not accurately model all temperature ranges, leading to inconsistencies between the numerical model and experimental results; and iii) the anisotropic nature of the material, particularly in the direction perpendicular to the semi-finished product, may also contribute to the differences observed between the simulation and the experimental model.

The evolution of the process temperature, as determined experimentally and through simulation, is illustrated in Fig. 8. The experimental temperature was measured using the thermography technique as the average value of a 10mm² area around the maximum point identified in the thermographic images. The temperature obtained from the simulation was extracted as the maximum value from the field of nodal temperature values.

The analysis of the temperature evolution in the process highlights the following aspects.

The temperature experimentally determined by the thermography technique presents a local periodic variation caused by the measurement system: the thermal imaging camera focuses on a lateral part and the base of the truncated cone, whose dimensions increase over time, and the tool passes only once through it during the execution of a planetary rotation around the symmetry axis of the part.

The temperature evolution curve exhibits a distinct pattern: it begins with an initial increase, followed by a relatively stable phase, which is somewhat similar to the progression of deformation forces.

At the start of the process, the temperature rises due to the significant amount of mechanical energy required to initiate plastic deformation, combined with the high intensity of friction between the tool and the blank. This friction occurs because of the substantial contact pressure during this initial stage. As the material transitions into the plastic domain, heat is generated through internal dissipation mechanisms associated with the deformation.

As the process continues, the temperature tends to stabilize. This stabilization occurs because mechanical energy dissipates more evenly, and the deformation and friction processes reach a state of thermal equilibrium. At this point, the rate of heat generation approximately equals the rate of heat dissipation into the environment and the tool.

The temperature evolution obtained by simulation has a relatively similar shape to that of the experimentally determined temperature. However, there are noticeable differences between their maximum values, with the simulated values being higher than those observed experimentally. The main reasons for these discrepancies are as follows: i) The adiabatic approach utilized in this model does not account for thermal conduction, which means it cannot incorporate heat exchange between the various elements in contact (such as the tool and base plate) during the simulation process. This largely explains why the temperatures predicted by the simulation are higher than those measured experimentally; ii) The use of oil lubrication in the experiments results in a temperature distribution that differs significantly from the scenario without lubrication, which was considered in the simulation; iii) Additionally, the analysis of the experimentally deformed parts revealed that small micro-chips occur on a local scale, which can also influence the global quantities analyzed through simulation.

The results previously analyzed indicate that the numerical model developed for simulating the incremental plastic deformation process with a tool demonstrates reasonable accuracy and can be validated.

To exploit the results of the numerical simulation, the following analyzes the relationship between deformation forces and temperature in the process. It is well-established that there is a direct correlation between these two factors: as deformation forces increase, the mechanical energy generated also rises, resulting in heat generation and, consequently, an increase in temperature. Conversely, elevated temperatures can reduce the forces required for deformation by enhancing the material's ductility, thus lowering its resistance to flow.

The analysis of the evolution of deformation forces and temperatures throughout the process, illustrated in Figure 7 and Figure 8, led to the identification of several "critical points" specific to the SPIF process:

- Point *a*: This point marks an inflection in the evolution of both deformation forces and temperature during the process.
- Point *b*: This point is associated with the onset of the stabilization process for the deformation force F_Z.
- Point b1: This point signifies the beginning of the stabilization process for the deformation forces F_X and F_Y.
- Point c_0 : This point corresponds to the start of the temperature stabilization process.
- Point c: This point indicates the end of the incremental plastic deformation process.

The 3D shape and the distribution of equivalent plastic strain (PEEQ) resulting from the numerical simulation related to these critical points are presented in Figure 9 and Figure 10, respectively. Additionally, the evolution of the height of the part is illustrated in Figure 11.

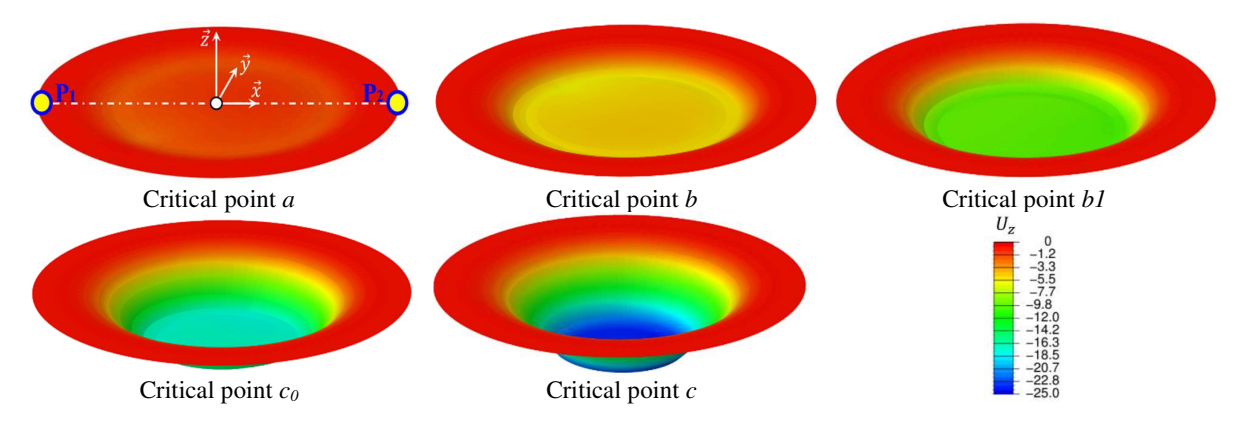


Fig. 9. The 3D shape of the deformed part associated with critical points in the process. The color code indicates the position of the points in the z-direction.

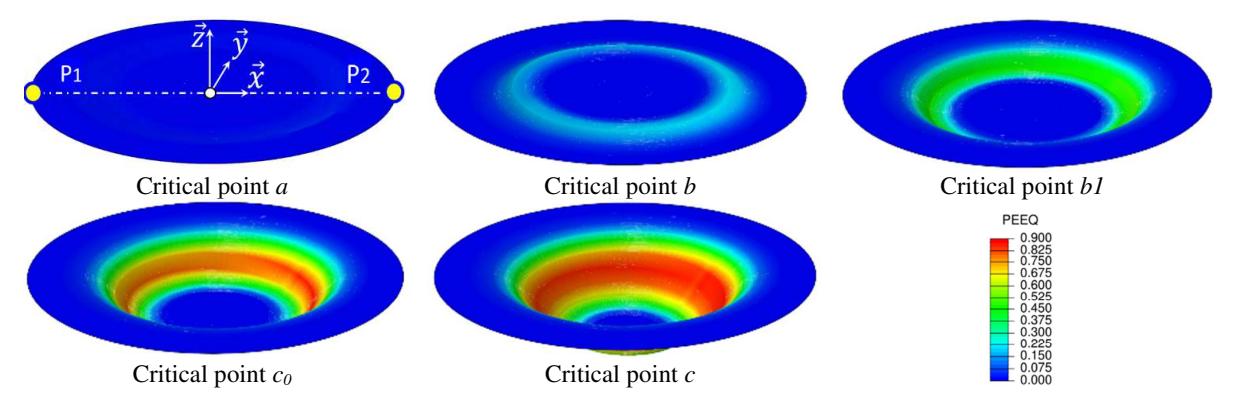


Fig. 10. The equivalent plastic strain (PEEQ) distribution for different critical points of the process.

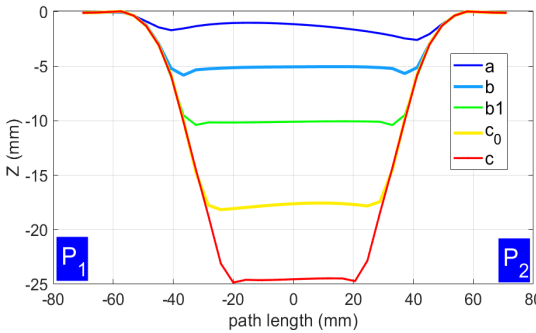


Fig. 11. Evolution of the height of the deformed part in relation to the "critical points" of the process.

The correlated analysis of the evolution of deformation forces, process temperatures, equivalent plastic strain (PEEQ) distribution, and the height of the deformed part allowed us to make the following observations regarding the development of the process:

- Up to the critical point a, the tool interacts with the undeformed material, which remains within the elastic range (PEEQ < 0.15). The friction between the tool and the material primarily occurs at the front part of the tool, and the height of the part does not exceed one-fourth of the tool's radius.
- As the material transitions into the plastic range (PEEQ > 0.15), the forces needed for deformation increase significantly, while its resistance diminishes. This leads to the deformation force F_Z stabilizing at a critical point, referred to as point b. This critical point b marks the beginning of the process of forming the side wall of the truncated cone, during which the sheet material is elongated
- The contact area between the tool and the workpiece continuously increases due to the interaction along the lateral edge of the workpiece. At the critical point, labeled as b1, the contact area approaches its maximum value. At this point, the tool begins to work with its entire active part, and the forces F_X and F_Y stabilize. The height of the formed part is equal to the tool's radius, which is 10 mm.
- The temperature in the process continues to increase significantly, even after the size of the contact surface between the tool and the workpiece has stabilized (critical point *b1*) because the plastic deformation process

generates heat through the internal dissipation mechanism.



Fig. 12. Image of the part incrementally deformed using a hemispherical head tool with radius R=10mm.

Starting from the critical point c_0 , the temperature in the process begins to stabilize. At this stage, mechanical energy is dissipated more uniformly, and the processes of deformation and friction reach thermal equilibrium. Between the critical points c_0 and c (the end of the process), the sheet material undergoes significant elongation, and the variable PEEQ exceeds 0.825 without breakage. demonstrated as experimentally in Fig. 12. During this phase, the rate of heat generation is approximately equal to the rate of heat dissipation to the environment and the tool.

5. CONCLUSION

The numerical model developed utilized the finite element method (FEM) and was implemented using ABAQUS software. The explicit method was chosen to focus on plastic deformation phenomena. To characterize the thermo-mechanical behavior of the material, the Johnson-Cook law was used, with parameters determined through experimental methods. An adiabatic approach was employed to model thermal phenomena. To optimize simulation time, a mass scaling strategy was implemented.

The numerical model was validated by comparing the deformation forces and temperatures from the simulation with those obtained through experimental methods. It was shown that:

- The evolution forms of the deformation forces and temperatures in the process obtained by simulation are similar to those obtained experimentally;
- There are differences between the maximum values of these quantities, with the values obtained through simulation being higher than those determined experimentally. This is why the main causes were highlighted.

The analysis of the evolution of deformation forces and temperatures throughout the process, along with the changes in the 3D shape and height of the part, as well as the distribution of equivalent plastic strain (PEEQ), provided insights into the development of the Single Point Incremental Forming process. This analysis helped identify critical points specific to the process: the beginning of plastic deformation in the workpiece, the beginning of the stabilization of deformation forces, and the beginning of the stabilization of temperature during the process.

Research can continue by enhancing the accuracy of the numerical model, analyzing the geometric precision of the part, and determining the optimal process parameters.

6. REFERENCES

- [1] Suresh, K., Regalla, S.P., Effect of Mesh Parameters in Finite Element Simulation of Single Point Incremental Sheet Forming Process, Procedia Materials Science, vol. 6, pp. 376–382, 2014, doi: 10.1016/j.mspro.2014.07. 048.
- [2] Suresh, K., Khan A., Regalla, S.P., *Tool path definition for numerical simulation of single point incremental forming*, Procedia Engineering, Elsevier Ltd, 2013, pp. 536–545. doi: 10.1016/j.proeng.2013.09.128.
- [3] Song, X., Zhang, J., Zhai, W., Taureza, M., Castagne, S., Danno, A., *Numerical and Experimental Study of Micro Single Point Incremental Forming Process*, Procedia Engineering, Elsevier Ltd, 2017, pp. 825–830. doi: 10.1016/j.proeng.2017.10.836.
- [4] Kumar, A., Critical state-of-the-art literature review of surface roughness in incremental sheet forming: A comparative analysis, Applied Surface Science Advances, vol. 23, Sep. 2024, doi: 10.1016/j.apsadv.2024.100625.
- [5] Duflou, J.R., Vanhove, H., Verbert, J., Gu, J., Vasilakos, I., Eyckens, P., *Twist revisited: Twist*

- phenomena in single point incremental forming, CIRP Ann Manuf Technol, vol. 59, no. 1, pp. 307–310, 2010, doi: 10.1016/j.cirp.2010.03. 018.
- [6] Nimbalkar, D.H., Nandedkar, V.M., Review of Incremental Forming of Sheet Metal Components, Int. Journal of Engineering Research and Applications, Vol. 3, Issue 5, Sep-Oct 2013, pp. 39-51, https://www.ijera.com/papers/_issue5/I353951.pdf.
- [7] Qin, Z., Gatea, S., Ou, H., Friction and heat partition coefficients in incremental sheet forming process, J Manuf Process, vol. 124, pp. 503–523, Aug. 2024, doi: 10.1016/j.jmapro. 2024.06.015.
- [8] Sharma, M., Bhattacharya, A., Paul, S.K., Explicating tensile response of AA6061-T6 sheet post single point incremental forming: Two camera-DIC strain measurement and texture analysis, Mechanics of Materials, vol. 192, May 2024, doi: 10.1016/j.mechmat.2024.104963.
- [9] Chang, Z., Yang, M., Chen, J., Geometric deviation during incremental sheet forming process: Analytical modeling and experiment, Int J Mach Tools Manuf, vol. 198, May 2024, doi: 10.1016/j.ijmachtools.2024.104160.
- [10] Chang, Z., Yang, M., Li, Y., Chen, J., Understanding a new wrinkling behavior of annular grooved panel during flexible free incremental sheet forming, J Mater Process Technol, vol. 333, Dec. 2024, doi: 10.1016/j.imatprotec.2024.118608.
- [11]Long, H., Peng, W. X., Chang, Z. D., Zhu, H., Jiang, Y. J., Li Z. H., New rosette tools for developing rotational vibration-assisted incremental sheet forming, J Mater Process Technol, vol. 326, May 2024, doi: 10.1016/j.imatprotec.2024.118311.
- [12] Hu, X., Li, Y., Liu, Y., Sun, X., Mo, X., Xue, F., Simulation, experiment and application of the damage analysis in the sheet plate forming based on modified Lemaitre model, Mater Today Commun, vol. 40, Aug. 2024, doi: 1.1016/j.mtcomm.2024.109715.
- [13] Khan, S., Pradhan, S. K., Experimentation and FE simulation of single point incremental forming, Materials Today: Proceedings, Elsevier Ltd, 2019, pp. 2334–2339. doi: 10.1016/ j.matpr.2019.09.123.
- [14] Ullah, S., Li, X., Li, D., Fast simulation of incremental sheet metal forming by multitooling, J Manuf Process, vol. 84, pp. 669–680, Dec. 2022, doi: 10.1016/j.jmapro.2022.10.025.
- [15] Zeradam, Y., Krishnaiah, A., Numerical Simulation and Experimental Validation of

- Thickness Distribution in Single Point Incremental Forming for Drawing Quality Steel, 2020, http://www.ripublication.com.
- [16] Jagtap, R., Bendure, S., Kumar, P., Sharma, A., Experimental and simulation studies on hybrid incremental sheet forming, Engineering Research Express, vol. 4, no. 2, Jun. 2022, doi: 10.1088/2631-8695/ac73df.
- [17] Lee, H. R., Lee, M. G., Park, N., Effect of evolutionary anisotropic hardening on the prediction of deformation and forming load in incremental sheet forming simulation, Thin-Walled Structures, vol. 193, Dec. 2023, doi: 10.1016/j.tws.2023.111231.
- [18] Vosniakos, G. C., Pipinis, G., Kostazos, P., *Numerical simulation of single point incremental forming for asymmetric parts*, Facta Universitatis, Series: Mechanical Engineering, vol. 19, no. 4, pp. 719–734, Dec. 2021, doi: 10.22190/FUME201210046V.
- [19] Chang, Z., Peng, W., Long, H., Towards understanding the surface friction in rotational-vibration assisted incremental sheet forming, J Mater Process Technol, vol. 336, Feb. 2025, doi: 10.1016/j.jmatprotec.2024.118692.
- [20] Zhao, X., Ou, H., A new flexible multi-point incremental sheet forming process with multi-layer sheets, J Mater Process Technol, vol. 322,

- Dec. 2023, doi: 10.1016/j.jmatprotec.2023. 118214.
- [21] Nirala, H. K., Agrawal, A., Adaptive increment based uniform sheet stretching in Incremental Sheet Forming (ISF) for curvilinear profiles, J Mater Process Technol, vol. 306, Aug. 2022, doi: 10.1016/j.jmatprotec.2022.117610.
- [22] Mezher, M. T., Shakir, R. A., Modelling and evaluation of the post-hardness and forming limit diagram in the single point incremental hole flanging (SPIHF) process using ANN, FEM and experimental, Results in Engineering, vol. 20, Dec. 2023, doi: 10.1016/j.rineng.2023. 101613.
- [23] ASM International, ASM Aerospace Specification Metals Inc. Aluminum 6061-T6; 6061-T651, http://asm.matweb.com/search/SpecificMaterial.asp?bassnum=MA6061t6.
- [24]Iordache, D.M., Oprescu, E.R., Malea, C.I., Niţu, E.L., Crăcănel, M.O., Bădulescu, C., Determination of Johnson-Cook material constants for Copper using traction tests and inverse identification, IOP Conf. Ser.: Materials Science and Engineering, 1182 (2021), doi: 10.1088/1757-899X/1182/1/012032

Cercetări privind modelarea numerică a procesului de deformare plastică incrementală cu ajutorul unei scule cu cap semisferic

Acest studiu prezintă modelarea numerică a procesului de deformare plastică incrementală cu ajutorul unei scule cu cap semisferic a unei table din aliaj de aluminiu AA6061. Modelul cu elemente finite (FEM) a fost dezvoltat în ABAQUS, folosind metoda explicită de analiză a deformației plastice. Comportamentul termo-mecanic al materialului a fost definit prin legea Johnson-Cook, modelarea fenomenelor termice s-a bazat pe o abordare de tip adiabatic, iar durata simulării a fost micșorată prin utilizarea mass scaling. Validarea, bazată pe compararea rezultatelor simulării cu forțele și temperaturile de deformare experimentale, a evidențiat tendințe similare, deși unele diferențe în valorile maxime au apărut din cauza ipotezelor de modelare. Analiza forțelor de deformare, a temperaturilor, a evoluției formei 3D și a deformării plastice echivalente (PEEQ) a oferit informații cheie asupra procesului SPIF. Au fost identificate puncte cheie în derularea procesului SPIF care marchează debutul deformării plastice, stabilizarea forțelor și temperaturii în timpul procesului.

- Emanuel BADULESCU, PhD student, National University of Science and Technology POLITEHNICA Bucharest. Doctoral School of Industrial Engineering and Robotics. emanuel.badulescu@stud.fiir.upb.ro; **RATEN** Institute for Nuclear Research, Mioveni. emanuel.badulescu@nuclear.ro
- **Daniela Monica IORDACHE**, PhD, Professor, National University of Science and Technology POLITEHNICA Bucharest, Pitesti University Center, Manufacturing and Industrial Management Department, daniela.c.iordache@upb.ro, 0348 453 160.
- **Eduard Laurențiu NIȚU**, PhD, Professor, National University of Science and Technology POLITEHNICA Bucharest, Pitesti University Center, Manufacturing and Industrial Management Department, eduard.l.nitu@upb.ro, 0348 453 159.
- Claudiu BĂDULESCU, PhD, Associate Professor, Researcher, UBS UBO ENSTA ENIB, UMR CNRS 6027, Research Institute Dupuy de Lôme (IRDL), Brest Cedex 9, France, claudiu.badulescu@ensta.fr.